# Detection of fractional steps in cargo movement by the collective operation of kinesin-1 motors

**Cécile Leduc, Felix Ruhnow, Jonathon Howard, and Stefan Diez***

Max Planck Institute of Molecular Cell Biology and Genetics, Pfotenhauerstrasse 108, D-01307 Dresden, Germany

Edited by James A. Spudich, Stanford University School of Medicine, Stanford, CA, and approved May 8, 2007 (received for review February 28, 2007)

**The stepping behavior of single kinesin-1 motor proteins has been studied in great detail. However, in cells, these motors often do not work alone but rather function in small groups when they transport cellular cargo. Until now, the cooperative interactions between motors in such groups were poorly understood. A fundamental question is whether two or more motors that move the same cargo step in synchrony, producing the same step size as a single motor, or whether the step size of the cargo movement varies. To answer this question, we performed *in vitro* gliding motility assays, where microtubules coated with quantum dots were driven over a glass surface by a known number of kinesin-1 motors. The motion of individual microtubules was then tracked with nanometer precision. In the case of transport by two kinesin-1 motors, we found successive 4-nm steps, corresponding to half the step size of a single motor. Dwell-time analysis did not reveal any coordination, in the sense of alternate stepping, between the motors. When three motors interacted in collective transport, we identified distinct forward and backward jumps on the order of 10 nm. The existence of the fractional steps as well as the distinct jumps illustrate a lack of synchronization and has implications for the analysis of motor-driven organelle movement investigated *in vivo*.**

collective motion | microtubules | nanometer tracking | quantum dots

Active cellular transport, such as organelle traffic, is driven by motor proteins of different families such as kinesin, myosin, and cytoplasmic dynein (1). On the level of single molecules, the stepping behavior of these motors has been studied in great detail *in vitro* (2–4). Although many motors within these families have been shown to be processive, meaning that individual motors are able to produce continuous motion (5–7), in cells, they usually operate in small groups (8–11). However, little is known about the possible mechanisms of coordination between such motors.

Kinesin-1 (henceforth denoted "kinesin") is a heterotetrameric motor enzyme that converts the chemical energy of ATP hydrolysis into mechanical work. A single motor moves with 8-nm steps (12) toward the plus end of microtubules (MTs). It translocates with an asymmetric hand-over-hand mechanism (13, 14) and performs ≈100 steps before detaching from the MT (5, 15, 16). The step size is independent of the force and the ATP concentration (17). When a small group of kinesins carries the same cargo, it is known that the run length increases with the number of motors (5, 15, 18). But what is the step size of such cargo movement? A number of recent studies reported the detection of 8-nm steps in the displacement of cellular cargo *in vivo* (19, 20). Although no detailed mechanism for the occurrence of these 8-nm steps, which correspond to the unit step size of single motor molecules, was elucidated, these findings are intriguing as they might suggest a synchronization of the motors (i.e., all of them stepping at the same time) involved in transport.

When studying collective effects in cargo transport by multiple motors, knowledge of the exact number of force generators is a key prerequisite. However, until now, the stepwise motion of kinesins was only investigated *in vitro* by using immobilized MTs and kinesin-coated microbeads (12, 17, 21, 43), motor-attached quantum dots (QDs) (3, 22, 23), or single fluorescently labeled motors (14, 24). Although extremely powerful for the study of single motors, such "stepping assays" have the disadvantage that it is difficult to determine unambiguously how many motors are producing the motion in the multimotor case. To circumvent this problem, we used an "upside-down" gliding motility assay (5, 42), where MTs were transported by fluorescently labeled kinesin motors attached to a glass surface. In this geometry, the glass surface played the role of the cargo, and the stepping motion of the MT corresponded to the relative motion of the cargo. Most importantly, the fluorescence signal of the motors, as well as a number of additional evidences, allowed us to unequivocally identify the number of motors working together in propelling the MT over the surface. In this article, we studied the stepping motion when one, two, three, and many ($n > 10$) kinesin motors simultaneously interacted with a MT.

## Results

The experimental setup is schematically depicted in Fig. 1*A*. His-tagged GFP-kinesin molecules were bound to the glass surface of a flow chamber via penta-His antibodies. Rhodamine-labeled, biotinylated MTs were incubated with streptavidin-coated QDs (25) and injected into the flow chamber. In addition, multicolored Tetraspeck fluorescent beads (diameter 200 nm, labeled with four distinct fluorophores) were fixed on the surface and used as references to correct for spatial drift. Images were collected at 10–20 frames per second by using total internal reflection fluorescence (TIRF) microscopy and analyzed by using a home-developed tracking software. Our imaging allowed for a spatial accuracy of 2.1 nm in the position of surface-immobilized QD and ≈3 nm for the tracking of QDs attached to motor-driven MTs [see *Methods* and supporting information (SI) *Appendix*]. Experiments were performed at low ATP concentration (≈0.3 $\mu$M) so that the speed was sufficiently slow to resolve steps as small as 4 nm in MT motion (see *Methods*). To estimate the number of motor molecules involved in the transport of individual MTs we imaged the MT and kinesin positions (Fig. 1*B*). Because, during the imaging, the MTs moved a significantly shorter distance than the spacing between individual kinesin molecules, it was possible to determine the number of motors that could potentially interact with the MT. However,

Author contributions: C.L. and S.D. designed research; C.L. performed research; F.R. and J.H. contributed new reagents/analytic tools; C.L. analyzed data; and C.L., J.H., and S.D. wrote the paper.

The authors declare no conflict of interest.

This article is a PNAS Direct Submission.

Freely available online through the PNAS open access option.

Abbreviations: MT, microtubule; QD, quantum dot; TIRF, total internal reflection fluorescence.

*To whom correspondence should be addressed at: Max-Planck-Institute of Molecular Cell Biology and Genetics, Pfotenhauerstrasse 108, 01307 Dresden, Germany. E-mail: diez@mpi-cbg.de.

This article contains supporting information online at www.pnas.org/cgi/content/full/0701864104/DC1.

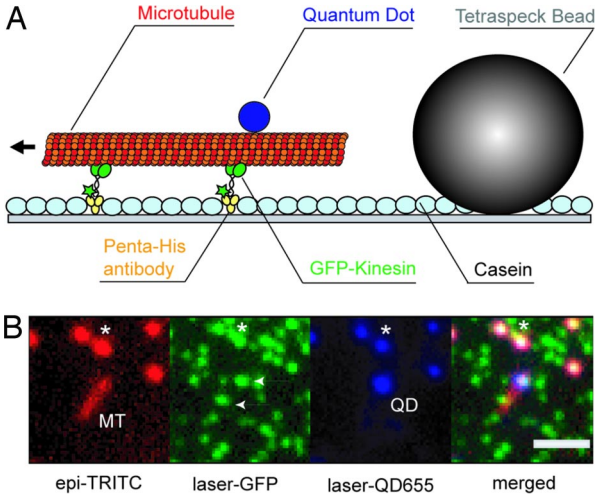


**Fig. 1.** Experimental setup of MT tracking by multicolor fluorescence microscopy. (*A*) Principle of an *in vitro* gliding motility assay. QD-coated MTs were propelled by His-tagged GFP-kinesin molecules that had been attached to the surface of a glass coverslip by Penta-His antibodies. The remainder of the surface was passivated by casein. The multicolored Tetraspeck fluorescent beads were used as references to correct for spatial drift. (*B*) Multicolor images of gliding motility. Rhodamine-labeled MTs were imaged by epi-fluorescence microscopy (epi-TRITC). The positions of the GFP-kinesins (laser-GFP) and the QDs (laser-QD655) were obtained by TIRF microscopy of the same field of view. The image on the right (merged) corresponds to the overlay of the three colors. The arrowheads show the kinesin positions in the laser-GFP image. The asterisk shows the appearance of two Tetraspeck beads in all colors. (Scale bar, 2 $\mu$m.)

because one or more GFP molecules could have been bleached before observation, we unambiguously checked the exact number of active motors using additional criteria as described below.

**One-Motor Case.** The swiveling of a MT around the point where it is attached to an individual kinesin molecule was used as the main criterion for single-motor movement (Fig. 2*A*) (5, 13, 26). The precise position of the kinesin molecule (cross in Fig. 2*A*) was determined from a circular fit of the QD positions during a time interval where the MT movement was negligible (*SI Appendix*). The relative distance of the tracked QD from this kinesin position was calculated as a function of time, and several intervals of this data are represented in Fig. 2*B* (red curve). Clear steps can be observed by eye and were analyzed with a step-finding algorithm (27) (black curve and numbers). The histogram of pair-wise distances (Fig. 2*C*), which represents the distribution of distances between any two points along the displacement trace in Fig. 2*B*, shows a periodicity of 8 nm. This periodicity is in good agreement with the data obtained from the step-finding algorithm.

Fig. 3*A* shows the histogram of extracted step sizes obtained from 11 individual QDs (382 steps) bound to 11 swiveling MTs. The first peak of a double-Gaussian fit (continuous line) of this histogram yielded a central value of $d_1 = 8.1 \pm 0.2$ nm. The second peak was constrained to be centered at twice the step size of the first peak to account for fast consecutive steps that could not be resolved with our time resolution. The histogram of the corresponding dwell times is presented in Fig. 3*B*. The distribution is well fit by a single-exponential rate constant of $k_1 = 0.49 \pm 0.03$ s$^{-1}$. This rate constant corresponds to a second order association rate $k_{on} \approx 0.49/0.3\ \mu M^{-1}\,s^{-1} = 1.6\ \mu M^{-1}\,s^{-1}$ in good agreement with previously published values (28) for a kinesin-1 motor that takes one step upon hydrolysis of one ATP molecule (28, 29) with a Poisson-distributed stepping rate at limiting ATP concentrations (30).

**Two-Motor Case.** MT swiveling could also be used to unambiguously determine when two motors moved a MT. The *x-y* trajectory of the QD shown in Fig. 2*D* contains two linear parts linked together by a swiveling part. Although the swiveling part is again indicative of only one motor interacting with the MT, we believe that exactly two kinesins carried the MT in the linear parts before and after the swiveling. Indeed, from fluorescence measurements, we estimated a kinesin density of ≈2 molecules per $\mu m^2$. Thus, it was very unlikely that a MT with a length of only a few microns would have interacted with more than two motors during the linear parts. Fig. 2*E* shows three different parts of the projected walked distance along the linear pathway of the QD (see *Methods*) as a function of time (Fig. 2*E*, red curve) during the two-motor regimes. Again, steps can be observed by eye and were analyzed with the step-finding algorithm (Fig. 2*E*, black curve and numbers). When multiple QDs bound to the same MT were tracked, coincidental stepping in time and step width were detected for a large number of steps. The histogram of pair-wise distances (Fig. 2*F*) reveals a structure with a periodicity of ≈4 nm, in agreement with the data obtained from the step-finding algorithm.

Fig. 3*C* shows the histogram of step sizes extracted by the step-finding algorithm obtained from 17 individual QDs (749 steps) bound to 16 MTs carried by two kinesins. As in the one-motor case, a double-Gaussian fit (Fig. 3*C*, continuous line) of this histogram was performed and yielded a central value of $d_2 = 4.2 \pm 0.1$ nm for the first peak. The histogram of the corresponding dwell times (Fig. 3*D*) was best fit by a single-exponential decay with $k_2 = 1.00 \pm 0.04$ s$^{-1}$.

For a Poisson stepper, the ratio of the velocity and the stepping rate should provide a second estimate of the step size. The average MT velocities were $v_1 = 4.3 \pm 0.5$ nm/s (mean ± SEM, $n = 11$), and $v_2 = 4.5 \pm 0.4$ nm/s ($n = 17$) in the one- and two-motor cases, respectively. Dividing by the respective stepping rates yields $v_1/k_1 = 8.8 \pm 1.7$ nm, and $v_2/k_2 = 4.5 \pm 0.9$ nm, in good agreement with our direct measurements of the step sizes.

**Multimotor Case.** To test whether distinct steps would still be observable in cases where a large number of motors interacted with the MT, we performed control experiments at a 100-fold increased kinesin concentration (see Fig. 2 *G–I*). In the traces of the walked distance (data from 20 MTs), no steps were detectable. Moreover, in the histogram of pair-wise distances, neither a periodic structure nor a peak at 0 nm was observed, confirming the absence of steps.

**Fluctuation Analysis.** To estimate the underlying step sizes without relying on any step-finding algorithm, we evaluated the statistical properties of our tracked data and compared them with the expected values for a Poisson stepper (see details in *SI Appendix*). An estimator of the step size $d$ is given by:

$$d = 6\,\frac{\langle y^2(t)\rangle_T}{x(T)} \qquad [1]$$

where $x(t)$ is the walked distance of a Poisson stepper at time $t$ during a total time interval of $T$. $y(t)$ is the deviation from the linearized movement where the speed of the stepper is estimated by: $x(T)/T$

$$y(t) = x(t) - \frac{x(T)}{T}\,t \qquad [2]$$

Using the same data as used for the histograms of Fig. 3, we calculated step sizes of $d_1^{calc} = 8.8 \pm 0.8$ nm in the one-motor case, and $d_2^{calc} = 4.1 \pm 0.3$ nm in the two-motor case. The same analysis for the many-motor case resulted in $d_{many}^{calc} = 0.73 \pm$

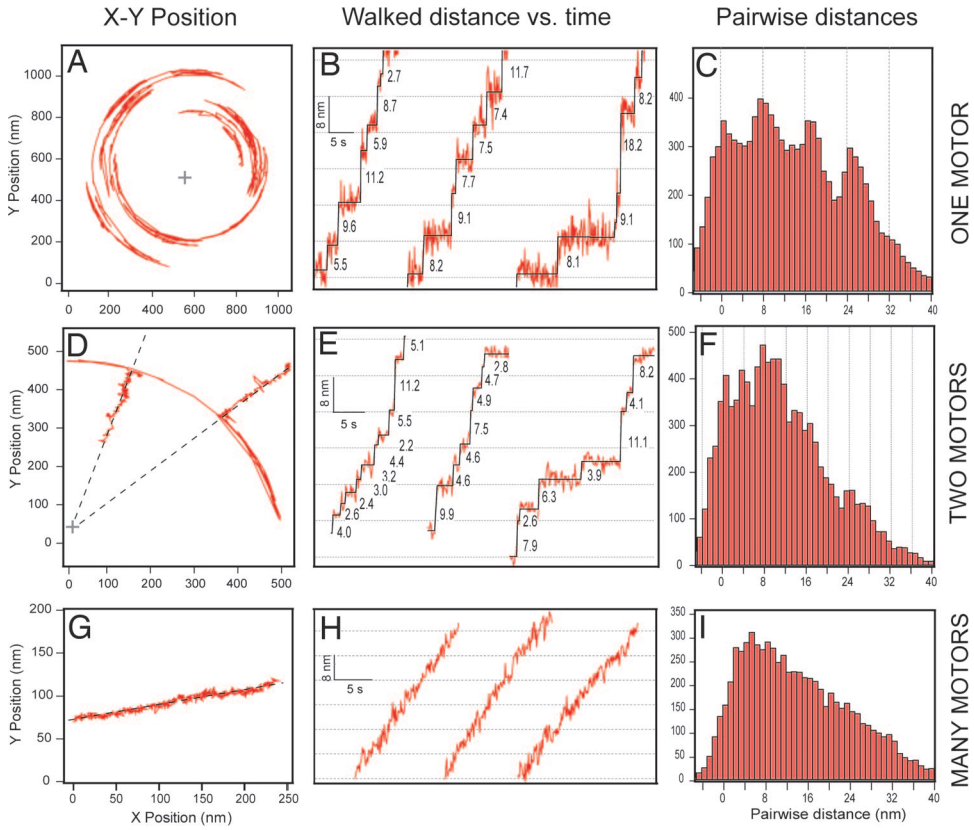


**Fig. 2.** Analysis of MT motion for one, two, and many motors operating collectively. (*A*, *D*, and *G*) *x*–*y*-trajectories of individual QDs bound to a MT for the one-motor case (*A*), the two-motor case (*D*), and the multimotor case (*G*). The crosses in *A* and *D* mark the positions of the kinesin molecules to which the MTs are attached during swiveling. (*B*, *E*, and *H*) Walked distance of the tracked QDs as a function of time (red curves) for three different time intervals from the depicted *x*–*y* trajectories. In *B*, the walked distance was derived from the relative distance of the tracked QD from the position of the kinesin molecule. In *E* and *H*, the walked distance was derived from the projection of the QD positions onto the dashed lines in *D* and *G*, indicating the fitted pathways of the MTs during linear movement. The black lines indicate the fitted steps as obtained from the applied step-finding algorithm, and the numbers indicate the step sizes in nanometers. (*C*, *F*, and *I*) Histograms of pair-wise distances ($d_i - d_j$ for $i \geq j$) calculated from 150 consecutive data points of the curves in *B*, *E*, and *H*, independently from the step-finding algorithm.

0.02 nm, confirming once again the absence of measurable steps. These findings provide a third independent check of the step sizes.

**Irregular Cargo Jumps.** During gliding motility assays with kinesin concentrations similar to the two-motor case, a number of longer MTs did not show any periods of one-motor swiveling. When analyzing the walked distance as a function of time (see Fig. 4) no uniform steps of any step size were detected. Instead, we noticed occasional irregular and distinct jumps with sizes on the order of 10 nm that were never present when the MTs were driven by one or two motors. From fluorescence imaging of the kinesin molecules in overlap with the MTs, we conclude that three motors were involved in active transport. To further characterize the nature of the irregular jumps, we analyzed the "sideways" movement of the QDs perpendicular to the direction of MT motion. Although we found the extent of the sideways motion to be a function of the density of transporting motors and the position of the QD along the MT (*SI Appendix*), we did not observe any pronounced irregularities associated with the jumps. We interpret the absence of large sideways motion as indicating that the MT moved on a straight path over the motors and that the jumps are associated with readjustments of the strain within the motors in the direction of the path of the MTs. In contrast, when a MT bent outwards ("buckled") between two transporting motors, a pronounced sideways motion was detected (*SI Appendix*). Intriguingly, the irregular jumps occurred in both forward and backward directions (Fig. 4*B*).

## Discussion

The presence of the fractional 4-nm steps observed in the two-motor case rules out the possibility of synchronization between the motors. Instead, we believe that the observed behavior can be explained by the mechanism presented in Fig. 5. Both motors are permanently fixed to the glass surface (i.e., the cargo) with their tail domains. When one motor (called the "advancing" motor) performs an 8-nm forward step, it is being stretched in the direction opposite to its motion. The MT, which is considered to be a stiff rod, then stretches the other "lagging" motor, which at that point in time, remains bound to the MT, as it is known for processive kinesins (2). The time that it takes the MT to transmit the force to the lagging motor in the viscous environment of the buffer solution can be calculated as the ratio of the drag coefficient of the MT and the stiffness of the motors (31). Assuming a drag coefficient of $10^{-5}$ pN s/nm for a 2-$\mu$m-long MT (32) and a motor stiffness of $\approx$0.5 pN/nm (33) yields a relaxation time well below 1 ms. Because this time constant is significantly shorter than our image acquisition time, we are not able to detect what occurs during the reestablishment of the force balance. Instead, we observe only the equilibrium states where the restoring forces exerted by the two motors on the filament are balanced. The motors, which are described to first approximation as identical springs, are stretched in opposite

BIOPHYSICS

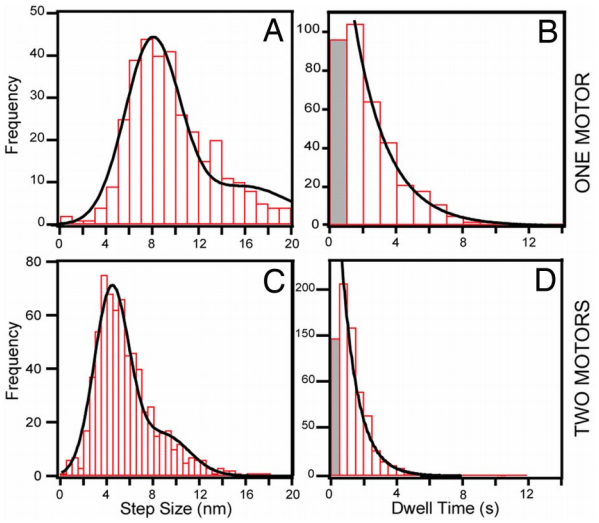


**Fig. 3.** Step sizes and dwell times of the tracked QDs. (*A* and *C*) Histograms of step sizes in the one-motor case (*A*) and the two-motor case (*C*). Data were obtained from 11 different QDs in *A* and 17 in *C*. The first peaks of double-Gaussian fits (solid lines) gave step sizes of $d_1 = 8.1 \pm 0.2$ nm in (A) and $d_2 = 4.2 \pm 0.1$ nm in *C*. (*B* and *D*) Histograms of the corresponding dwell times. The solid lines represent the exponential fit of the dwell time distribution weighted by the square root of the count in each bin (41) (equal to the standard deviation) which gave $k_1 = 0.49 \pm 0.03\ s^{-1}$ (reduced $\chi^2 = 0.4$; 10 degrees of freedom) in *B* and $k_2 = 1.00 \pm 0.04\ s^{-1}$ (reduced $\chi^2 = 1.5$; 9 degrees of freedom) in *D*. The low numbers of events in the very first bins of the dwell-time histograms (gray shaded bins) result from the difficulty of detecting steps that are in the range of (or shorter than) the camera acquisition time. Consequently, we omitted these data in the exponential fits. We note that the number of these missed events corresponds well to the number of nonresolvable ''double-steps'' (16 nm for the one-motor case and 8 nm for the two-motor case) in the step-size histograms.

directions, and the projected sum of their deformations should equal zero. Note that this behavior is independent of the absolute amount of strain accumulated in each motor. Thus, whenever one motor performs an 8-nm step, this distance is shared between the two motors equally, giving rise to successive 4-nm displacements of the MT.

Even though the motors do not synchronize, they might still coordinate such that the stepping of one motor would influence

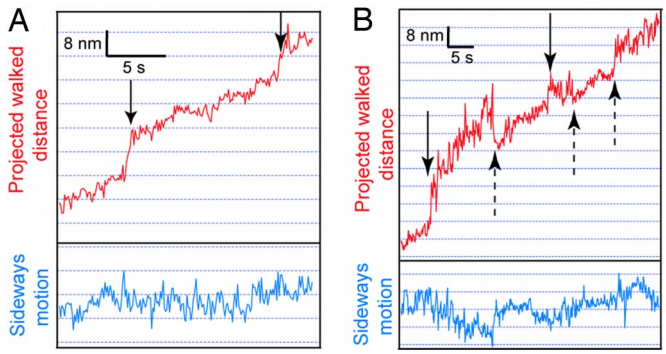


**Fig. 4.** Distinct jumps in the MT displacement in the three-motor case. (*A* and *B*) Projected walked distances of two QDs (red curves) and the corresponding sideways motion (blue curves). The arrows point to the presence of jumps in the forward (solid line) and the backward (dashed line) direction. That exactly three motors were involved in transport was inferred from: (*i*) the multicolor fluorescent images where three green spots were in overlap with the MT and (*ii*) the fact that, if only two of those were active, we would expect the pronounced existence of 4-nm steps, which we did not observe.

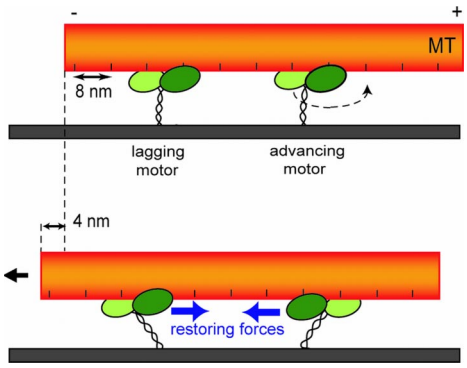


**Fig. 5.** Schematic diagram of a gliding MT in the two-motor case. When one motor performs an 8-nm step, the final displacement of the QD-coated MT is 4 nm.

the stepping of the other one. The advancing motor, which feels a force in the opposite direction of its movement, might be expected to have a decreased probability of making the next step (34, 35). On the other hand, the lagging motor, which is stretched in the direction of its movement, feels a restoring force that might, to some extent, increase the probability of that motor to make a step. In other words, the connection between the motors might cause them to alternate, with one motor stepping after the other. Such coordination between the motors should lead to a dwell-time distribution that is not describable by a single exponential decay [as in the case of head coordination for Myosin V (36, 37)]. However, our data (Fig. 3*D*) was best fitted by a single exponential decay with a stepping rate equal to twice the stepping rate of a single kinesin ($k_2 \approx 2k_1$). This shows that there was no overall strong coordination, in the sense of a strict alternation, present between the investigated motors despite their truncated contour length as well as their strong coupling by means of the glass surface and the stiff MT. As such, our findings are, moreover, in agreement with the fact that MT motility driven by multiple kinesin motors goes at the same velocity as single-motor-driven gliding (5), showing that internal loads are not sufficient to decrease the net forwards gliding rate. Nevertheless, whereas there must be some coordination between the motors when they are both fully stretched to their contour length (i.e., when neither one of them can be further strained), the sensitivity of our method might not be sufficient to detect the contribution of such rare events. Note that the hydrolysis cycle of kinesin can well be influenced by load at high and low ATP concentrations (34). We therefore believe that our results, albeit obtained at conditions where ATP binding to kinesin is rate limiting, also bear significance for collective motor transport at intracellular ATP concentrations.

In the three-motor case, we did not observe any uniform steps. Although steps with a length of 8/3 nm $\approx$ 2.7 nm would be expected for the collective operation of three Hookian spring-like motors, the force-extension curve of a single kinesin molecule will rather resemble that of a worm-like chain, i.e., stiffening up at longer elongations. Consequently, the stepping of a motor that is under more strain than the other motors in contact with the MT will lead to an overproportionally long step. In contrast to the two-motor case, where the motors always equally share the strain, the step sizes in the three-motor case are thus expected to vary between 0 and 8 nm, depending on the strain of the individual motor before performing the step.

The irregular jumps that we observed in the three-motor case are unlikely to be the result of multiple, temporally unresolved, fractional steps. First, the likelihood of approximately four fractional steps with an average step size of 2.7 nm ($4 \times 2.7$ nm $\approx$ 10 nm) occurring within 100 ms of camera exposure is extremely

small ($P < 2 \times 10^{-7}$), and second, backward jumps were also detected. We rather attribute the observed jumps to the detachment of a motor that had previously been strongly stretched. Such detachments are expected to readily occur for motors with limited processivity and will lead to jumps of any size between a portion of the fractional step size to many fractional step sizes. Thereby the magnitude of a jump will depend on the amount of strain accumulated in the strongly stretched motor before it detaches, and the direction of the jump will depend on whether this motor had previously performed more or fewer steps than the other ones. In fact, the maximum jump size should correspond to the length of a fully stretched motor divided by the number of remaining bound motors. Estimating a contour length of 20 nm for the truncated GFP-kinesin used in our experiments, this explains the 10-nm jumps in the three-motor case and the absence of detectable jumps in the many-motor case (Fig. 2*H*). The occurrence of the irregular jumps in the cargo position relative to the MT is a second manifestation of the lack of a strong coordination between the motors and suggests that meticulous care should be taken when analyzing the motion of intracellular cargo by nanometer tracking. Backward jumps could be mistaken as the operation of motors with opposite directionality, and forward jumps might suggest unexpectedly high cargo velocities in the forward direction.

In this article, we study the collective behavior of kinesin motors as they move along a MT. Although cases with many motors ($n \gg 1$) might exhibit a variety of additional cooperative phenomena (38), we focused on scenarios relevant to intracellular cargo transport by a small number (one, two, and three) of motors. We observed 8-nm steps when only one kinesin moved on a MT and fractional 4-nm steps of the cargo when two motors acted in concert. These step sizes were obtained by three independent methods based on step finding, kinetic analysis, and fluctuation analysis. The existence of fractional steps indicates that multiple kinesin motors do not synchronize under our experimental conditions (low ATP concentration and absence of external load). Moreover, analysis of the dwell-time distribution showed that the motors step stochastically, without any detectable coordination among each other. With regard to formerly reported substeps in the motion of molecular motors, our observations suggest that extreme prudence should be taken when interpreting stepping data from experiments where the involvement of a second motor in transport cannot be fully ruled out. Although, in our study, the motors keep a fixed relative position on the glass surface, they are less rigidly coupled to each other by means of the fluid surface of an organelle during *in vivo* transport. This difference might be one explanation for the 8-nm steps recently observed in intracellular vesicle transport (19, 20). On the other hand, our data might explain why those 8-nm steps are not consistently observed *in vivo*; they may indicate rather rare times of single molecule activity, or that load may synchronize multiple motors.

## Methods

**Gliding Assays with GFP-Kinesin and QD-Coated MTs.** We used truncated, GFP-labeled kinesin-1 constructs ($\text{rkin430}_{\text{GFP}}$), which contained the first 430 aa of kinesin-1 fused to a GFP and a His-tag at the tail domain (39). Rhodamine-labeled MTs were polymerized from 5 $\mu$l of bovine brain tubulin (4 mg/ml, mix of 1 biotin labeled/10 rhodamine labeled/189 unlabeled tubulin units; Cytoskeleton, Denver, CO) in BRB80 buffer [Pipes (pH 6.9)/1 mM EGTA/1 mM $MgCl_2$) with 4 mM $MgCl_2$, 1 mM Mg-GTP, and 5% DMSO at 37°C. After 5 min, MTs were stabilized and 100-fold diluted into room-temperature BRB80 containing 10 $\mu$M taxol and sheared four times to get short MTs (length $<5$ $\mu$m). Gliding motility assays were performed at room temperature in flow cells (final volume of $\approx 10$ $\mu$l) made of two silanized (dichlorodimethylsilane; Sigma, Taufkizchen, Germany) glass coverslips and heated Parafilm for sealing. The flow sequence was as follows (all of the chemicals except where specifically mentioned were purchased from Sigma): (*i*) the flow cell was filled with a solution of TetraSpeck microspheres (0.2 $\mu$m diameter from Mo Bi Tec) diluted 10-fold in BRB80. (*ii*) After 2 min, the solution was exchanged with a BRB80 solution containing penta-His antibodies (Qiagen, Hilden, Germany) at 20 $\mu$g/ml for high-kinesin-concentration assays and 0.2 $\mu$g/ml for low-kinesin-concentration assays. (*iii*) After 5 min, the surface was blocked with a solution of casein (from bovine milk, 0.5 mg/ml in BRB80) for 5 min to prevent nonspecific protein binding. (*iv*) GFP-labeled kinesin (10 $\mu$g/ml $\text{rkin430}_{\text{GFP}}$, 0.2 mg/ml casein, and 10 $\mu$M Mg-ATP in BRB80) was incubated for 5 min to bind the motors specifically to the antibodies by their His-tags. (*v*) QDs [1 $\mu$l of streptavidin-coated QDs, 655 nm emission; Quantum Dot Corporation (Hayward, CA), diluted 80-fold in BRB80] were first incubated for 5 min with 2 $\mu$l of biotinylated MTs (labeling each of the MTs with $\approx$1 QD) and then mixed with 47 $\mu$l of motility solution containing 10 $\mu$M Taxol, 0.2 mg/ml casein, 1 mM Mg-ATP, and an oxygen-scavenger system (40 mM D-glucose, 0.040 mg/ml glucose oxidase, 0.016 mg/ml catalase, and 20 mM DTT). The resulting MT–QD solution was injected into the flow cell, and unhindered gliding motility was verified. For that, each recording was preceded by an experiment at 1 mM ATP (saturating ATP), when the gliding velocity was fast enough to be measured within less than 1 min. We found average velocities of MTs with and without QDs of $v_{\text{with}} = 0.68 \pm 0.06$ $\mu$m/s (mean $\pm$ SD, $n = 15$) and $v_{\text{without}} = 0.68 \pm 0.07$ $\mu$m/s ($n = 15$) at 1 mM ATP, indicating a negligible impact of the QDs. (*vi*) The flow cell was rinsed with a motility solution containing 0.3 $\mu$M ATP and an ATP-regenerating system (2 mM creatine phosphate, 2 units/ml creatine kinase) and sealed with Vitrex.

**Image Acquisition by TIRF Microscopy.** Images were acquired on an Axiovert 200M microscope (Zeiss, Oberkochen, Germany) with a 100x (NA 1.45) oil-immersion objective, a Zeiss-TIRF slider, and a Micromax BFT 512 back-illuminated frame-transfer CCD camera (Photometrics, Tucson, AZ) or an Andor Ixon DV 897 (Andor, Belfast, U.K.). The pixel size in the acquired images was 130 nm (Micromax) or 160 nm (Andor). In some experiments a $\times 1.6$ magnifying optovar, which reduced the pixel size was used. Fluorescence excitation was provided by a mixed gas argon-krypton laser (Innova 70C Spectra; Coherent, Santa Clara, CA) or Hg-arc lamp. The following filter sets (Chroma Technology, Rockingham, VT) were used: TRITC (exc 535/50, em 610/75, dc 565 LP) for the rhodamine-labeled MTs, GFP (exc 488/10, em 515/30, dc 505 LP) for the GFP-kinesin and QD-655 (exc 488/10, em 660/50, dc 505 LP) for the QDs. A MetaMorph imaging system (Universal Imaging, Downingtown, PA) was used for data acquisition and primary data processing. First, the positions of the slowly moving MTs were recorded by using epi-fluorescence microscopy (epi-TRITC in Fig. 1*B*). Second, the kinesin molecules (laser-GFP, arrows point to the individual motors in Fig. 1*B*) were localized by TIRF imaging without any previous illumination to avoid bleaching of the GFP molecules. Consequently, the positions of MT-attached QDs were recorded as a function of time in TIRF mode (laser-QD655, streams of 1,000 frames, 100-ms exposure time each under continuous laser illumination). Because the reference beads were fluorescent in all three channels, it was possible to superimpose precisely the images of the rhodamine-labeled MTs, the GFP-labeled kinesins, and the QDs (merged). As the emission wavelength of the QDs was in the far red (655 nm), the contribution of the fluorescence coming from the dimly rhodamine-labeled MT was negligible.

**Nanometer Tracking of QDs.** The QD positions were tracked with nanometer accuracy by using a home-developed tracking software based on MatLab (MathWorks, Natick, MA) and two-dimensional Gaussian fits. For analysis, we used all tracked QD positions where the fluorescence intensity collected on the CDD chip corresponded to a flux of at least 500 photons per 100 ms at the centroid pixel, i.e., where photon shot noise was the principal source of noise. Thereby, we disregarded the data points of QDs in low-emission phases because of blinking in the analyzed trajectories. The theoretical tracking accuracy is then given by $(s^2/N)^{0.5}$, where $s^2$ is the variance obtained from the Gaussian fit and $N$ the number of collected photons (40). In our experiments, we found the Gaussian width $s$ to be ≈140 nm and the average number of collected photons originating from one QD to be 4,500 per 100-ms exposure. The resulting calculated accuracy then yields 2.1 nm per frame in good agreement with the width of the Gaussian distribution determined from tracking a surface-immobilized QD (*SI Appendix*). The tracking accuracy of QDs bound to gliding MTs was slightly reduced to ≈3 nm mainly because of Brownian motion of the MT-QD complex (*SI Appendix*).

**Step Analysis.** By using IGOR PRO 5.0 (WaveMetrics, Portland, OR): (*i*) the average position of five TetraSpeck beads was subtracted from the tracked positions of the QDs for drift correction, (*ii*) the pathways of the QDs were determined in the *x*–*y* plane after linear fits of the *x* position vs. time and the *y* position vs. time, and (*iii*) the QD positions were projected along the pathway to deduce the projected walked distance and the sideways motion. For swiveling MTs, bound to single motor molecules, the walked distance was calculated as the distance from the central kinesin position. Step analysis was performed by using an algorithm written in MatLab kindly provided by J. Kerssemakers and described in ref. 27. This algorithm assumes that the steps are hidden in Gaussian-distributed noise but makes no assumption on either step size or dwell time. The overall accuracy in step finding was tested by using piezo-based control measurements and allowed us to reliably discriminate steps as small as 4 nm (see *SI Appendix*).

We thank R. Cross (Marie Curie Institute, Surrey, U.K.) for the plasmid of the rkin430-GFP; C. Bräuer for protein purification; B. Nitzsche for experimental help; J. Kerssemakers (Max Planck Institute of Molecular Cell Biology and Genetics) for the step-finding program; E. Schaeffer and S. Grill for comments on an earlier version of the manuscript; and O. Campàs for illuminating discussions. Zeiss generously lent us the TIRF slider. This work was supported by German Federal Ministry of Education and Research Grant 03 N 8712) and the Max-Planck-Society.

1. Howard J (2001) *Mechanics of Motor Proteins and the Cytoskeleton* (Sinauer, Sunderland, MA).
2. Carter NJ, Cross RA (2006) *Curr Opin Cell Biol* 18:61–67.
3. Reck-Peterson SL, Yildiz A, Carter AP, Gennerich A, Zhang N, Vale RD (2006) *Cell* 126:335–348.
4. Sellers JR, Veigel C (2006) *Curr Opin Cell Biol* 18:68–73.
5. Howard J, Hudspeth AJ, Vale RD (1989) *Nature* 342:154–158.
6. Mehta AD, Rock RS, Rief M, Spudich JA, Mooseker MS, Cheney RE (1999) *Nature* 400:590–593.
7. King SJ, Schroer TA (2000) *Nat Cell Biol* 2:20–24.
8. Schuchardt I, Assmann D, Thines E, Schuberth C, Steinberg G (2005) *Mol Biol Cell* 16:5191–5201.
9. Levi V, Serpinskaya AS, Gratton E, Gelfand V (2006) *Biophys J* 90:318–327.
10. Ashkin A, Schutze K, Dziedzic JM, Euteneuer U, Schliwa M (1990) *Nature* 348:346–348.
11. Gross SP, Tuma MC, Deacon SW, Serpinskaya AS, Reilein AR, Gelfand VI (2002) *J Cell Biol* 156:855–865.
12. Svoboda K, Schmidt CF, Schnapp BJ, Block SM (1993) *Nature* 365:721–727.
13. Hua W, Chung J, Gelles J (2002) *Science* 295:844–848.
14. Yildiz A, Tomishige M, Vale RD, Selvin PR (2004) *Science* 303:676–678.
15. Block SM, Goldstein LS, Schnapp BJ (1990) *Nature* 348:348–352.
16. Hackney DD (1995) *Nature* 377:448–450.
17. Nishiyama M, Higuchi H, Yanagida T (2002) *Nat Cell Biol* 4:790–797.
18. Klumpp S, Lipowsky R (2005) *Proc Natl Acad Sci USA* 102:17284–17289.
19. Kural C, Kim H, Syed S, Goshima G, Gelfand VI, Selvin PR (2005) *Science* 308:1469–1472.
20. Nan X, Sims PA, Chen P, Xie XS (2005) *J Phys Chem B* 109:24220–24224.
21. Busoni L, Dupont A, Symonds C, Prost J, Cappello G (2006) *J Phys Condensed Matter* 18:S1957–S1966.
22. Seitz A, Surrey T (2006) *EMBO J* 25:267–277.
23. Courty S, Luccardini C, Bellaiche Y, Cappello G, Dahan M (2006) *Nano Lett* 6:1491–1495.
24. Vale RD, Funatsu T, Pierce DW, Romberg L, Harada Y, Yanagida T (1996) *Nature* 380:451–453.
25. Dahan M, Levi S, Luccardini C, Rostaing P, Riveau B, Triller A (2003) *Science* 302:442–445.
26. Hunt AJ, Howard J (1993) *Proc Natl Acad Sci USA* 90:11653–11657.
27. Kerssemakers JW, Munteanu EL, Laan L, Noetzel TL, Janson ME, Dogterom M (2006) *Nature* 442:709–712.
28. Schnitzer MJ, Block SM (1997) *Nature* 388:386–390.
29. Hua W, Young EC, Fleming ML, Gelles J (1997) *Nature* 388:390–393.
30. Yildiz A, Forkey JN, McKinney SA, Ha T, Goldman YE, Selvin PR (2003) *Science* 300:2061–2065.
31. Sekimoto K, Tawada K (1995) *Phys Rev Lett* 75:180–183.
32. Hunt AJ, Gittes F, Howard J (1994) *Biophys J* 67:766–781.
33. Kawaguchi K, Uemura S, Ishiwata S (2003) *Biophys J* 84:1103–1113.
34. Block SM, Asbury CL, Shaevitz JW, Lang MJ (2003) *Proc Natl Acad Sci USA* 100:2351–2356.
35. Carter NJ, Cross RA (2005) *Nature* 435:308–312.
36. Rief M, Rock RS, Mehta AD, Mooseker MS, Cheney RE, Spudich JA (2000) *Proc Natl Acad Sci USA* 97:9482–9486.
37. Veigel C, Schmitz S, Wang F, Sellers JR (2005) *Nat Cell Biol* 7:861–869.
38. Julicher F, Prost J (1995) *Phys Rev Lett* 75:2618–2621.
39. Rogers KR, Weiss S, Crevel I, Brophy PJ, Geeves M, Cross R (2001) *EMBO J* 20:5101–5113.
40. Thompson RE, Larson DR, Webb WW (2002) *Biophys J* 82:2775–2783.
41. Taylor JR (1997) *An Introduction to Error Analysis* (University Science Books, Basingstoke, Hampshire, UK), 2nd Ed.
42. Malik F, Brillinger D, Vale RD (1994) *Proc Natl Acad Sci USA* 91:4584–4588.
43. Gelles J, Schnapp BJ, Sheetz M (1988) *Nature* 331:450–453.